buildings

Article

Key Design Parameters Analysis and Calculation Theory Research on Bending Performance of Steel–UHPC Lightweight Composite Deck Structure

Jun Luo [1], Lingyun Zheng [1], Bida Pei [2,3,*], Yi Wang [4,*], Hanfei Yan [5] and Jun Zhao [1]

[1] School of Mechanics and Safety Engineering, Zhengzhou University, Zhengzhou 450001, China
[2] Key Laboratory of Bridge Engineering Safety Control by Department of Education, Changsha University of Science & Technology, Changsha 410114, China
[3] School of Civil Engineering, Changsha University of Science & Technology, Changsha 410114, China
[4] Henan Workman Construction Engineering Co., Ltd., Zhengzhou 450047, China
[5] School of Civil Engineering, Zhengzhou University, Zhengzhou 450001, China
* Correspondence: peibida@csust.edu.cn (B.P.); Chinawangyi@aliyun.com (Y.W.)

Abstract: This paper aims to study the influence of key design parameters (e.g., reinforcement ratio, cover thickness, stud spacing, and thickness of the ultra-high-performance concrete (UHPC) layer) on the longitudinal and transverse bending performance, as well as the cracking load and ultimate bearing capacity calculation theory of steel–UHPC lightweight composite deck (LWCD) structure. Four transverse bending tests and four longitudinal bending tests on steel–UHPC composite plates and steel–UHPC composite beams were conducted, respectively. The refined finite element models of components with different key design parameters based on ABAQUS were established. The influences of different key design parameters on the transverse and longitudinal flexural behaviors (e.g., load-mid-span displacement curve, cracking stress, stiffness, elastic limit load, critical slip load, ultimate bearing capacity and ductility) were compared and analyzed in detail. The ultimate bearing capacity can be improved by increasing the thickness of UHPC layer and the reinforcement ratio of longitudinal reinforcement, and reducing the cover thickness and the spacing of studs. According to the longitudinal bending characteristics of the steel–UHPC lightweight composite deck structure, the calculation formulas for the cracking load and the ultimate bearing capacity of the steel–UHPC composite beam are proposed, and the calculated values are in good agreement with test results (the errors are basically within 10%), which is convenient for practical engineering applications.

Keywords: steel–UHPC lightweight composite deck; design parameters; calculation theory; bending performance; crack width

check for updates

Citation: Luo, J.; Zheng, L.; Pei, B.; Wang, Y.; Yan, H.; Zhao, J. Key Design Parameters Analysis and Calculation Theory Research on Bending Performance of Steel–UHPC Lightweight Composite Deck Structure. *Buildings* **2023**, *13*, 504. https://doi.org/10.3390/buildings13020504

Academic Editor: Elena Ferretti

Received: 6 January 2023
Revised: 1 February 2023
Accepted: 8 February 2023
Published: 13 February 2023

1. Introduction

To fundamentally solve the issues (e.g., fatigue cracking and damage of asphalt overlay) of the orthotropic steel bridge deck, based on the previous research ideas of replacing the traditional asphalt pavement with concrete or other new materials [1–4], Shao et al. [5] proposed the LWCD structure in 2010. Figure 1 shows the cross-sectional dimension of a long-span steel bridge deck. Along the transverse direction, the composite plate composed of the steel panel and the UHPC layer generates a negative bending moment under the action of the wheel load on the U-rib. The section's neutral axis is in the UHPC layer, and its surface has the risk of cracking due to the large tensile stress [6–8].

At present, some experiments have been performed to investigate the bending behaviors or fatigue behaviors of UHPC members [9,10] and UHPC-NC composite beams [11–13]. The results indicated that a UHPC layer can improve the ultimate loads, stiffness, and cracking behaviors significantly. Moreover, scholars have conducted some research on the flexural properties, fatigue properties, and interface connection methods of LWCD structure. Zhang et al. [14] conducted an experimental study on the flexural and tensile strength of LWCD, and found that the flexural and tensile strength of the deck is much larger than the tensile stress under the design load and has a large safety reserve. Shao et al. [5] took the Humen Bridge as the background and conducted full-scale tests and theoretical analysis on LWCD. The results showed that the interface between the steel deck and the UHPC layer has strong shear resistance, and can be affected by wheel loads. The lower steel panel stress is significantly reduced. Pei et al. [15] conducted field test experiments on LWCD structure before and after laying the UHPC layer, and found that after laying the UHPC layer, the fatigue detail stress reduction in the steel panels, longitudinal ribs, transverse diaphragms, and other positions is more obvious, the biggest drop is 75%. In addition, many scholars have also studied the initial stiffness, cracking stress, ultimate bearing capacity and other mechanical properties of the composite structure by parameters, such as UHPC layer thickness and reinforcement ratio. Choi et al. [16] concluded that increasing the thickness of the UHPC layer could significantly improve the ultimate bearing capacity of the inverted T-steel–UHPC composite beams and delay the appearance and propagation of cracks. Li et al. [17] conducted a four-point bending negative moment bending test on a steel–UHPC composite simply supported plate and concluded increasing the reinforcement ratio can significantly improve the structure's transverse bending and tensile performance. The research of Liao et al. [18] showed that increasing the number of studs can improve the combined effect between the steel panel and the UHPC layer, thereby improving the overall stiffness of the steel–UHPC composite panel. Luo et al. [19,20] conducted a negative moment bending test on the steel–UHPC composite structure by changing the UHPC layer thickness, steel fiber type, reinforcement ratio, and other parameters to explore the influence of main design parameters on cracking stress, ultimate bearing capacity, crack spacing, etc. In addition, the crack width calculation theory is proposed. Wang et al. [21] conducted a negative bending moment test on steel-ultra-thin UHPC composite panels and found that the diameters and reinforcement ratio of steel bars have a greater impact on the nominal cracking stress of components. In contrast, the thickness of steel panels has a relatively small impact on it. Furthermore, the finite-element modeling (FEM) of composite bridge deck connections have been presented to define the crucial factors affecting the response of bridge hybrid deck panel system under monotonic loads [22]. Tzouka. E. et al. [23] studied the push-out performance of shear connectors via FEM. KMIECIK. P. et al. [24] studied the modeling method of reinforced concrete structures and composite structures. Liao et al. [18] built a comprehensive non-linear finite element (FE) analysis model through the software ABAQUS and the factors that influence the flexural performance of the steel–UHPC composite slabs (e.g., the ultimate capacity, the flexural stiffness, and the deflection) were analyzed.

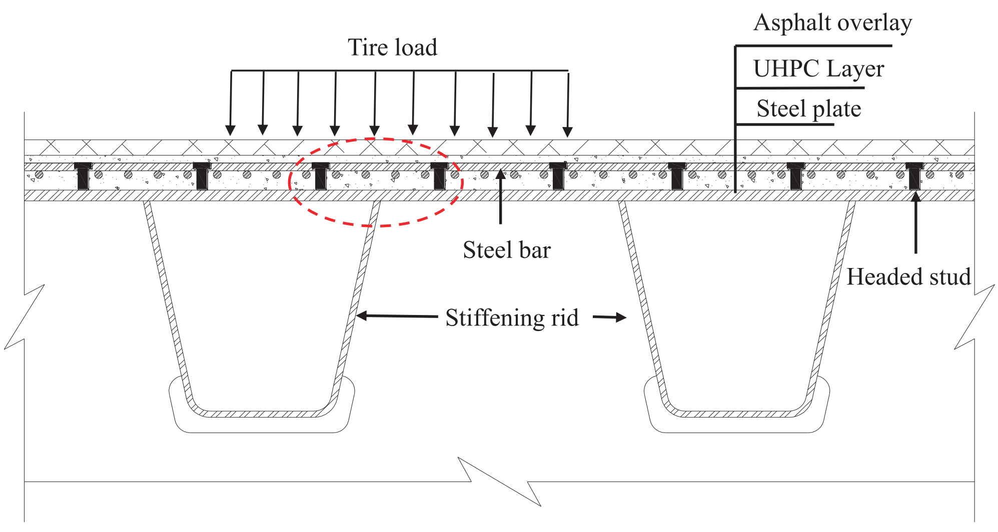

Figure 1. Schematic diagram of wheel riding U-rib.

However, the above studies are mostly experimental methods, the number of components is limited, and the influence of design parameters, such as UHPC layer thickness, stud spacing, and reinforcement ratio on the longitudinal and lateral bending performance of steel–UHPC composite structures, especially U-ribs, has not been systematically verified. There are few reports on the effects of thickness and steel panel thickness on the flexural performance of steel–UHPC composite beams. Therefore, based on the experimental tests and finite element analysis method, this paper aims to study the influence of key design parameters (e.g., reinforcement ratio, cover thickness, stud spacing and thickness of ultra-high-performance concrete (UHPC) layer) on the longitudinal and transverse bending performance, as well as the cracking load and ultimate bearing capacity calculation theory of steel–UHPC lightweight composite deck (LWCD) structure.

2. Experimental Program

2.1. Test Model Preparation

The steel–UHPC composite plate member comprises four parts: UHPC layer, steel panel, single-layer longitudinal and transverse reinforcement mesh, and studs. The steel–UHPC composite beam member is composed of UHPC layer, steel panel, U-rib, diaphragm, stud, and single-layer vertical and horizontal steel mesh. The design parameters of each component are shown in the Table 1 below. In component ID, S represents composite slab and U represents composite beam.

Table 1. Design parameters of steel–UHPC composite slab and composite beam.

Component ID	Design Parameters			
	Stud Spacing (mm)	**UHPC Layer Thickness (unit:mm)**	**Protective Layer Thickness (mm)**	**Longitudinal Reinforcement Number (n) [1]**
S150-60	150	60	/	/
S200-45-15-6	200	45	15	6
S150-60-15-4	150	60	15	4
S150-60-25-6	150	60	25	6
U155-45-15-12	155	45	15	12
U155-45-25-12	155	45	25	12
U155-60-15-12	155	60	15	12
U155-60-25-12	155	60	25	12

[1] The longitudinal reinforcement spacing of the composite slab is 200/n (mm), and the longitudinal reinforcement spacing of the composite beam is 600/n (mm).

The lateral force of the steel–UHPC lightweight composite deck structure can be simplified as a composite slab composed of a steel panel and a UHPC layer. In contrast, the longitudinal force can be simplified as a composite beam composed of an orthotropic steel bridge deck and a UHPC layer.

Multiple UHPC cubes (100 mm × 100 mm × 100 mm) and prisms (100 mm × 100 mm × 400 mm and 100 mm × 100 mm × 300 mm) were cast and cured at the same conditions of the steel–UHPC composite plate and beam specimens) to determine the compressive strengths, the flexural strengths, and the elastic modulus of the UHPC material, respectively. UHPC materials are selected from the special materials for steel bridge decks developed by Hunan University. According to the Chinese standard of UHPC [25], the compressive strength is 165 MPa, the elastic modulus is 45.8 GPa. Based on the measured data of the UHPC prisms and the method recommended by AFNOR [26], the corresponding tensile strength was about 9.0 MPa for the UHPC in this study. Q345qC steel is used, with a nominal yield strength of 345 MPa. The rebars adopt HRB400 reinforcement with a diameter 10 mm and nominal yield strength of 400 MPa.

Figure 2 shows a structural layout of the steel–UHPC composite slab test specimen (take S150-60-25-6 as an example). The rest of the composite slab test specimens are similar, except for the combination of four main parameters: UHPC layer thickness, stud spacing, number of longitudinally reinforcements, and cover thickness.

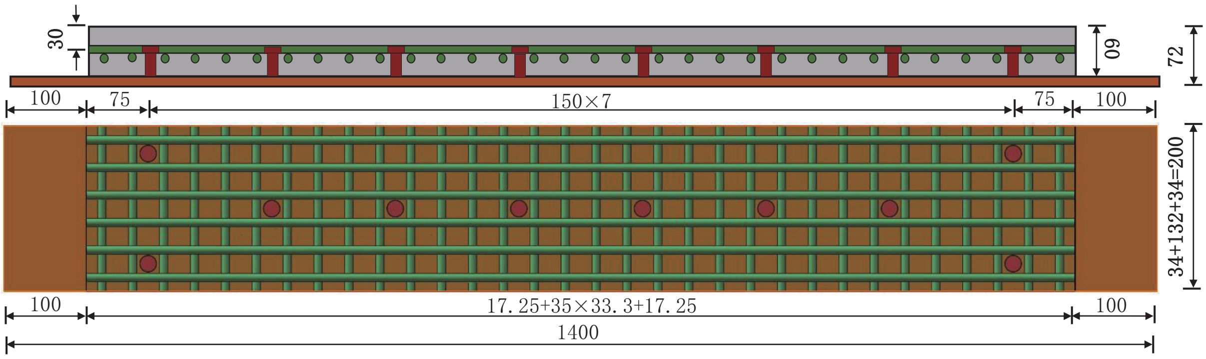

Figure 2. Structural layout of the steel–UHPC composite slab test specimen (unit: mm).

Figure 3 is a schematic diagram of the structure of part of the composite beam. The total length of the composite beam is 2100 mm, the width is 620 mm, the thickness of the steel plate is 12 mm, the thickness of the U-shaped stiffener is 6 mm, and the spacing of the stud is 155 mm. The rest of the composite beam test specimens are similar, only differing in the combination of three main parameters: UHPC layer thickness, longitudinal reinforcement number, and protective layer thickness. Among them, the adjacent studs are evenly arranged in the longitudinal direction, and the materials used are the same as the steel–UHPC composite slab.

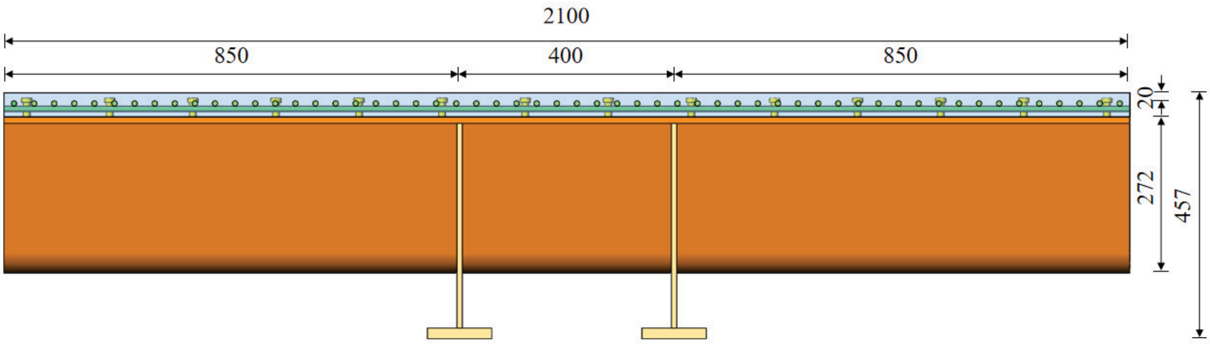

Figure 3. Schematic diagram of the structure of steel–UHPC composite beam test specimen (unit: mm).

2.2. Test Loading and Test Program

The composite beam and slab adopt the four-point loading method with a negative moment. Figure 4 is a schematic diagram of the loading of the composite slab test: the clear span of the slab between the two loading points is 1000 mm, the load is symmetrical, and the distance between the supports is 400 mm. D1∼D5 measure the deflection of the composite plate and solve the mid-span displacement according to the formula $d_p = D_{p3} - \frac{D_{p1}+D_{p5}}{2}$. Among them, D_{p3} is the measured mid-span displacement, and D_{p1} and D_{p5} are the absolute values of the displacement at the support. S1 and S2 measure the relative slip between the steel plate and the UHPC layer. Several strain gauges are evenly arranged on the upper surface of the longitudinal bars within the 400 mm pure bending section of each member. The specimen is loaded in two steps: first, the force loading mode with a loading amplitude of 2 kN/*level* is adopted, and when the elastic limit load of the component is about to be reached (referring to the inflection point of the component from elastic deformation to plastic development), it is converted into displacement-controlled loading.

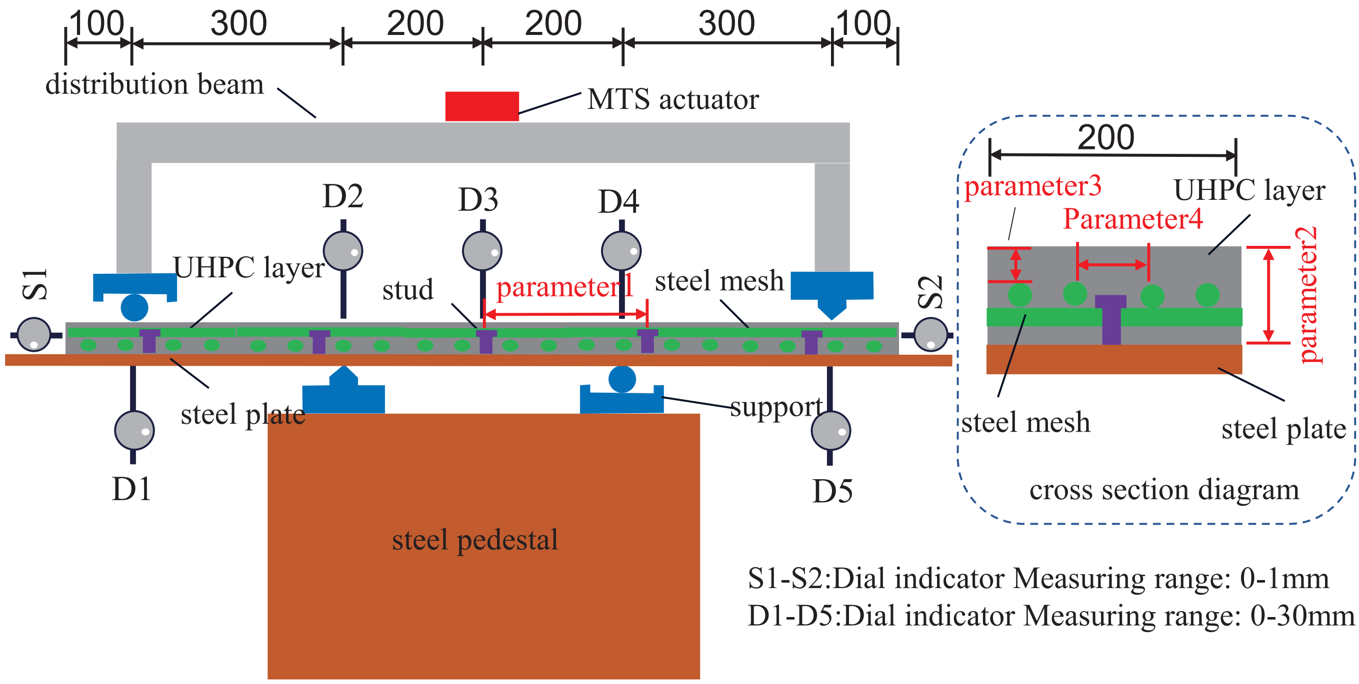

Figure 4. Test setup and layout of the displacement sensors.

2.3. Test Results

The photographs of failed reinforced steel–UHPC composite slab and composite beam specimens are shown in Figure 5. The crack distribution of the specimen after failure can be clearly seen from the photographs. The load-mid-span displacement curves of some members are shown in Figures 6 and 7. It can be seen that the reinforced steel–UHPC composite slab and composite beam roughly go through three stages:

(1) In the linear elastic stage, the structural stiffness remains unchanged, and no cracks occur during the test.
(2) In the crack propagation stage, the stiffness of the composite slab gradually decreases and enters non-linearity, which is accompanied by the appearance and expansion of surface cracks in the UHPC layer of the pure bending section. Different from the composite slab, the stiffness of the composite beam is not reduced at this stage, and the stiffness degrades significantly only when it is about to reach the yield state. This is because the global stiffness of the steel–UHPC composite beam is relatively large, the stiffness contribution rate of the UHPC layer is much lower than that of the UHPC layer in the composite slab, and the number and width of cracks are relatively small. Due to the bridging effect of steel fibers, the UHPC layer can continue to work, that is, the occurrence of cracks has little effect on the stiffness reduction in composite beams.
(3) In the yield stage, for the composite slab, the load increases slowly, and the displacement increases rapidly, and then the bearing capacity remains unchanged or shows a downward trend. At this stage, the number of cracks does not increase, but the width of cracks increases rapidly. For the composite beam, after the load reaches the peak value, the bearing capacity decreases rapidly with deflection, the number of cracks gradually increases, and the width gradually increases. At the same time, the cracks on the side of the UHPC layer continue to develop toward the bottom of the beam.

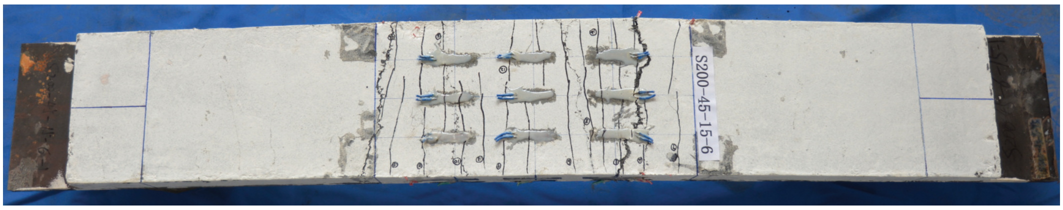

(**a**) Composite slab after failure (take S200-45-15-6 as an example).

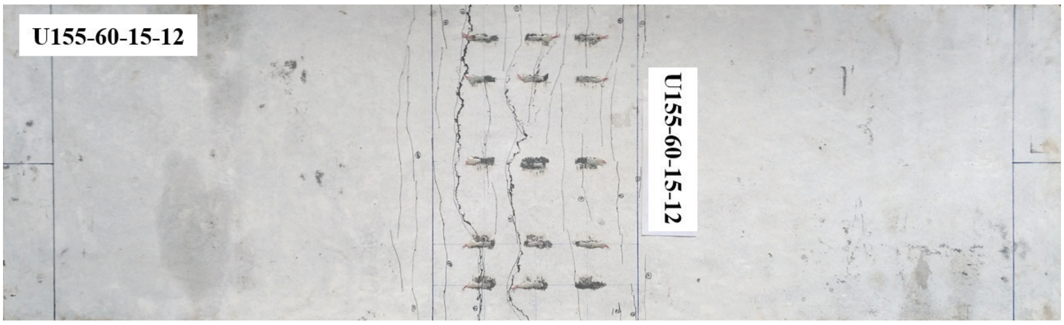

(**b**) Composite beam after failure (take U155-60-15-12 as an example)

Figure 5. Specimens after failure.

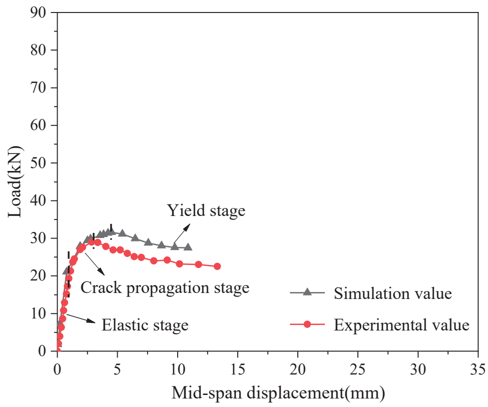

(**a**) S150-60.

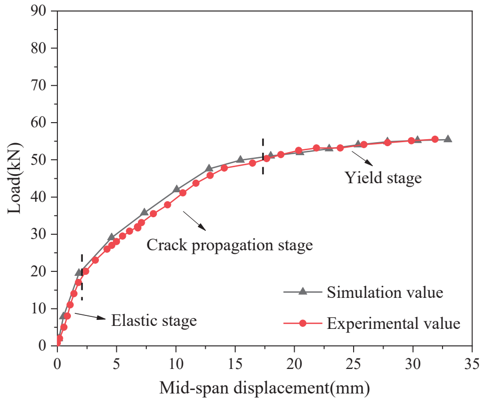

(**b**) S200-45-15-6.

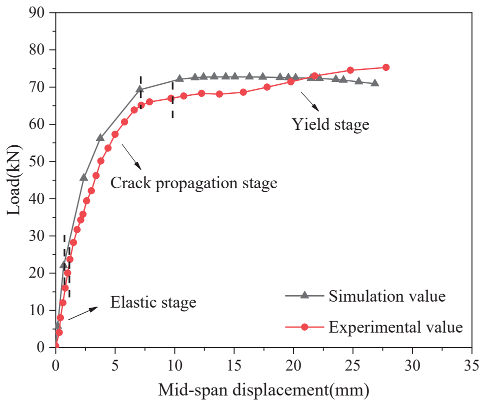

(**c**) S150-60-15-4.

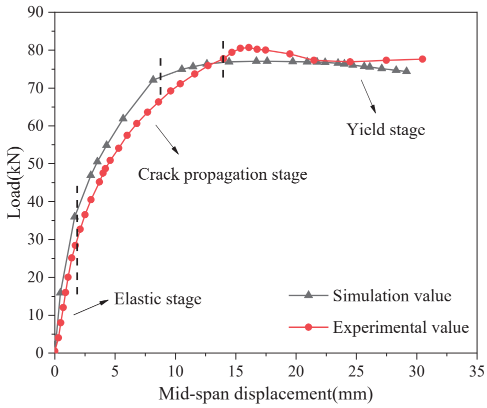

(**d**) S150-60-25-6.

Figure 6. Load-mid-span displacement curve of composite slab.

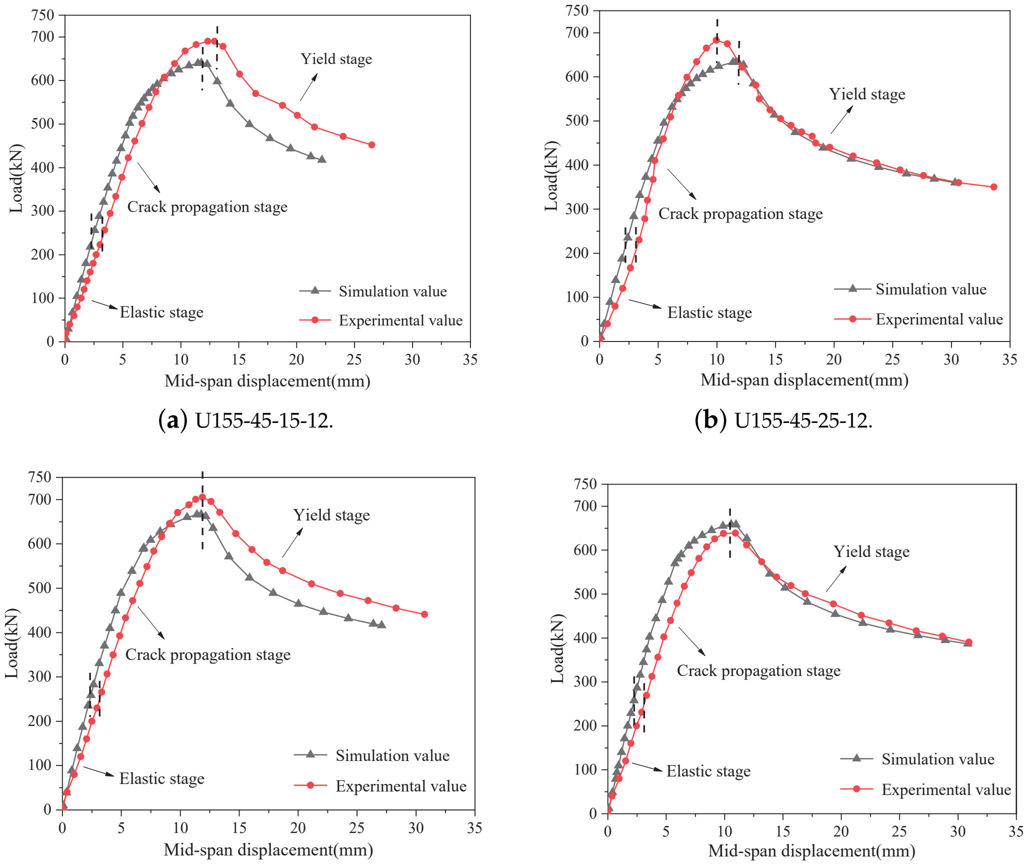

(**a**) U155-45-15-12. (**b**) U155-45-25-12.

(**c**) U155-60-15-12. (**d**) U155-60-25-12.

Figure 7. Load-mid-span displacement curve of composite beam.

3. Finite Element Analysis

3.1. The Establishment of Finite Element Model

This section takes the finite element modeling of composite beams as an example to illustrate the finite element model modeling process of steel–UHPC lightweight composite bridge deck structures.

(1) Constitutive relation

The UHPC material in the finite element analysis in this paper adopts the CDP model (Concrete Damaged Plasticity model) [27]. Because the CDP model considers the difference in tensile and compressive properties of materials, and takes tensile cracking and compressive collapse as the criteria for simulating concrete failure, which can well describe the inelastic behavior of brittle materials, such as concrete [28–30]. The non-linearity of concrete is simulated using the CDP model, which is defined in two parts: (I) Elastic stage, define UHPC elastic modulus E_s = 45.8 GPa, Poisson's ratio = 0.2; and (II) Damage plastic stage, the plastic parameters, uniaxial compressive stress–strain relationship, and uniaxial tensile stress–strain relationship of the material are defined. The plastic parameter values given in this paper are shown in Table 2. To improve the convergence of the calculation, the viscosity coefficient is taken as 0.003.

Table 2. UHPC Plastic failure criterion parameters.

Expansion Angle	Eccentricity	f_{b0}/f_{c0}	K	Viscosity Coefficient
36°	0.1	1.16	0.6667	0.003

Yang et al. [31] carried out the axial compression test of UHPC materials, obtained a stable compressive stress–strain whole process curve, and established the UHPC axial compression constitutive relationship. The tension constitutive relation adopts the UHPC axial tension constitutive model proposed by Zhang et al. [9]. In Figure 8a, the peak strain of UHPC $\varepsilon_0 = 3500\ \mu\varepsilon$, the compressive strength of UHPC $f_c = 165$ MPa. In Figure 8b, the tensile strength of UHPC $f_t = 9$ MPa, the peak strain in elastic stage $\varepsilon_{t0} = 196\ \mu\varepsilon$, the ultimate strain $\varepsilon_{tp} = 3000\ \mu\varepsilon$.

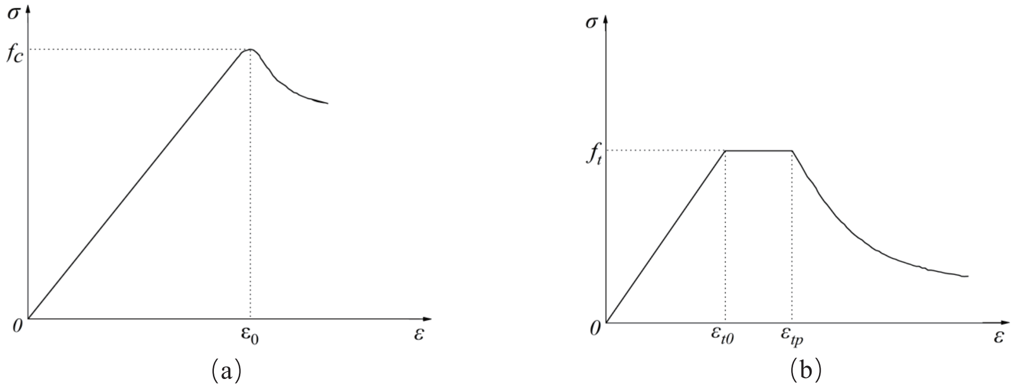

Figure 8. Constitutive relation curve of UHPC: (**a**) stress–strain relation for compression, (**b**) stress–strain relation for tension.

The elastic residual energy generated by stress acting on damaged or non-destructive materials is the same, so when solving damaged materials, the elastic modulus can be replaced by the damaged elastic modulus of the material.

The elastic residual energy W_d^e of the non-destructive material is:

$$W_d^e = \frac{\sigma^2}{2E_0} \tag{1}$$

In the formula, σ is the UHPC uniaxial stress.

The elastic energy W_d^e of the lossy material is:

$$W_d^e = \frac{\bar{\sigma}^2}{2E} \tag{2}$$

$$\bar{\sigma} = (1-d)\sigma \tag{3}$$

In the formula, $\bar{\sigma}$ is the effective stress, E is the unloaded elastic modulus of UHPC after damage, d is UHPC damage factor.

From Equations (1)–(3), the calculation formula of d is deduced:

$$d = 1 - \sqrt{\frac{E}{E_0}} = 1 - \sqrt{\frac{\sigma}{E_0\varepsilon}} \tag{4}$$

In the formula, ε is the UHPC uniaxial strain.

The compressive and tensile stress–strain relationships of UHPC obtained in the previous section are put into the above formula, and the damage factor values of UHPC under compressive and tensile states can be calculated. The constitutive relations of the steel panel and the reinforcement are all based on the ideal elastic–plastic model: the steel plate is Q345 steel commonly used in bridges, with elastic modulus $E_s = 206$ GPa, yield strength $f_y = 345$ MPa and Poisson's ratio $\rho = 0.3$. Rebar grade is HRB 400, the diameter is 10 mm, $f_y = 400$ MPa, Poisson's ratio $\rho = 0.3$, the constitutive relationship is shown in Figure 9.

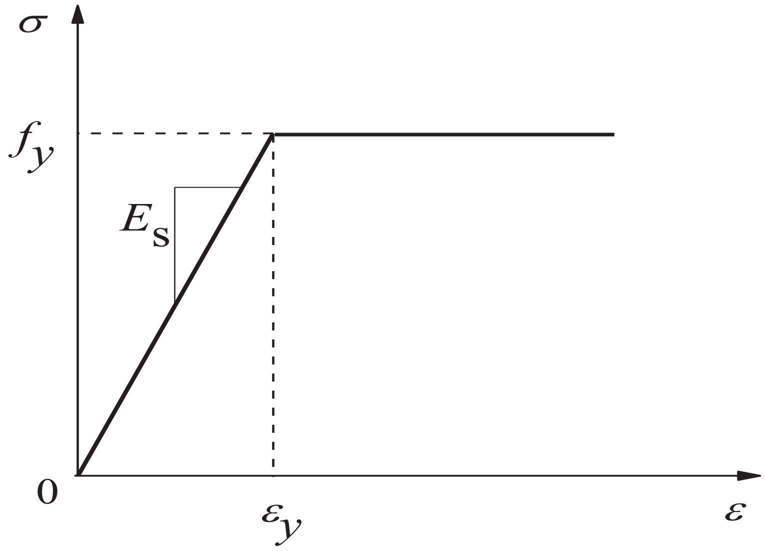

Figure 9. Steel stress–strain relation curve.

The elastic–plastic (hardening) constitutive model is used for studs, and its stress–strain relationship is generally simplified into a three-line model. The modulus of elasticity of the stud $E_s = 206$ GPa, yield strength $f_y = 375$ MPa, and ultimate strength $f_u = 450$ MPa. The stress–strain relationship curve of the stud is shown in Figure 10.

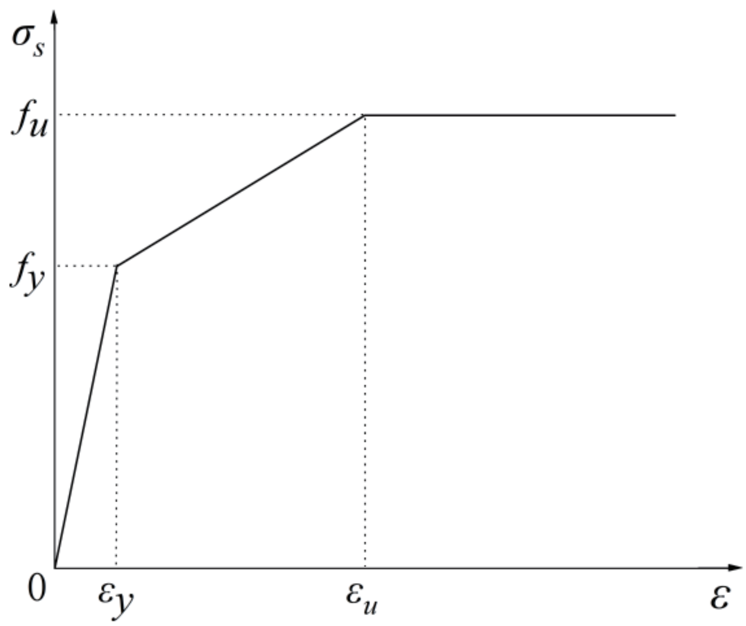

Figure 10. Stud stress–strain relationship curve.

(2) Element type selection

C3D8R elements simulate UHPC layers and studs, and longitudinal and transverse reinforcement mesh is simulated by T3D2 elements. Since the dimensions of the steel panel and U-rib along the thickness direction are much smaller than those of the other two directions, in order to reduce the amount of calculation, a four-node quadrilateral linear reduced-integral shell element S4R is used to simulate [32]. The diaphragm in the test mainly plays the role of facilitating loading and transferring the load, so the stiffness of the diaphragm is set to be much greater than that of the test beam, taking $E_s = 206$ GPa, to ensure that the finite element analysis process itself will not deform, and the shell element S4R is used for simulation. To prevent abnormal local stress concentration or excessive deformation of the UHPC layer during the non-linear analysis process, which may cause deviations in the calculation results, a support pad was set at the boundary conditions of the UHPC layer, and the C3D8R element was used to simulate its stiffness. The settings are the same as for the diaphragm.

(3) Simulation of interface contact

To reduce constraints and save calculation time, the steel panels, U-ribs, and diaphragms are set as a whole. The contact method between the UHPC layer and the steel panel is "surface-to-surface contact". The tangential direction adopts the penalty function, the friction coefficient is 0.4, and the normal direction adopts hard contact, the bottom of the stud is "bound" on the steel panel, and the stud body is "embedded" in the UHPC layer. The support pads are "bound" to the surface of the UHPC layer, and the longitudinal and transverse reinforcement meshes are "embedded" in the UHPC layer. The loading method of the finite element model is displacement loading, and the support is set as a hinge support, that is, one side is restricted by $U1 = U2 = U3 = 0$, and the other layer is restricted by $U1 = U2 = 0$.

(4) Meshing

After the mesh sensitivity analysis, the mesh size of the calculation model is as follows: UHPC layer, steel panel, U-rib, and diaphragm all use 30 mm global size; vertical and horizontal reinforcement meshes use 50 mm global size, studs use 2 mm global size, and pads use 40 mm global size. The composite beam model after meshing is shown in Figure 11.

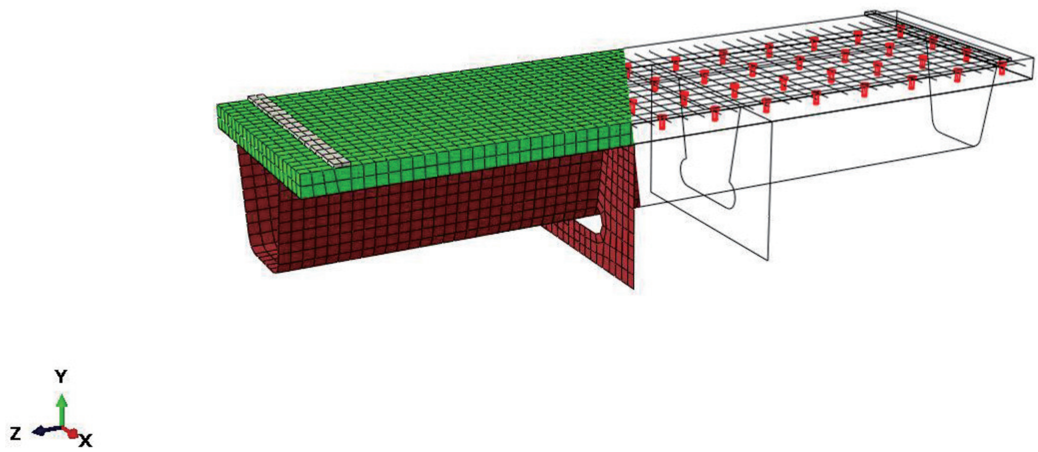

Figure 11. Meshing of composite beam finite element model and distribution of reinforcement frame and stud.

The material constitutive relations of the composite slab finite element model are the same as those used for the steel–UHPC composite beam. The simulation of interface contact and element types of the composite slabs are the same as for composite beams. However, the meshing of composite slabs is different from that of composite beams. The steel panel of the composite slabs adopt a global size of 8 mm, and a 2 mm local seed is set in the area welded to the stud. The UHPC layer adopts an 8 mm global size, and the area in contact with the stud is 2 mm local seeds. The studs adopt a 2 mm global size, and a 1 mm local seed is set in a small area where the stud body is close to the steel panel to avoid grid distortion caused by stress concentration. The reinforcement adopts 15 mm global size. The composite slab model after meshing is shown in Figure 12.

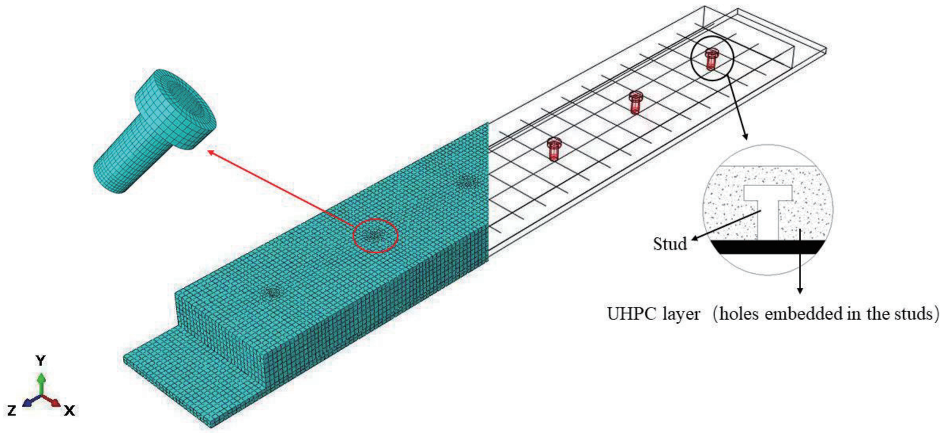

Figure 12. Meshing of composite slab finite element model and distribution of reinforcement frame and studs.

3.2. Load-Mid-Span Displacement Curve

Figures 6 and 7 compare the the load-mid-span displacement curves of the steel–UHPC composite slabs and composite beams obtained from the finite element analysis and test, respectively. It shows that the finite element model established in this paper can more accurately predict the force behavior of components during the loading process.

For the composite slab, in the elastic stage and the crack propagation stage, the curve slopes of the finite element analysis and the test results of the components are the same; that is, the stiffness of the finite element model is in good agreement with the stiffness of the test specimen. For reinforced members, the ultimate bearing capacity of the finite element analysis is slightly lower than the test results. The reasons are that: on the one hand, the steel fibers in the UHPC in the test members are randomly distributed, which can prevent concrete cracking and crack development, but the finite element software cannot simulate the crack resistance of the steel fiber in the UHPC; on the other hand, the actual strength of the steel used for the rebars and steel panel of the test member is greater than its standard strength, and the strength of the steel can increase to a certain extent after tensile yield; while in the finite element analysis, after the rebars yield, with the increase in the load, the strength of the reinforcement can only be stabilized at 400 MPa.

For the composite beam, the structural stiffness calculated by the model is slightly larger than the experimental value. The reason may be that the micro-cracks and shrinkage of the UHPC under the influence of the external environments are not considered in the finite element simulation. It is regarded as a homogeneous mass, and there is a certain difference between the constitutive relationship of the material and the actual one. However, the test specimens may have initial defects during the processing.

3.3. Load–Rebar Stress Curve

Extract each member's average value of longitudinal reinforcement stress within the range of 400 mm pure bending section and draw a load–reinforcement stress curve, as shown in Figures 13 and 14. The finite element analysis agrees with the load–rebar stress curve obtained from the test. For the steel–UHPC composite beam, the stress of the rebar increases slowly at the initial loading stage. After the specimen enters the plastic development stage, the rebar plays a significant role, and the stress increases rapidly until reaches the yield strength of 400 MPa. After the rebar yields, the specimen enters the yield stage. At different stages, the steel stress and load are linear. The reason for the sudden change of the steel stress curve in the finite element analysis results in the figure is: the constitutive relationship of the rebar set by the author in the ABAQUS finite element software is an ideal elastic–plastic model, so after the rebar yields, as the load continues to increase, the rebar stress is no longer caused by an increase. For the steel–UHPC composite beam, in the initial loading stage, the reinforcement stress increases linearly with the load. After entering the crack propagation stage, the growth rate of the reinforcement stress gradually accelerates, and the reinforcement stress has a nonlinear relationship with the load. Unlike the steel–UHPC composite slab, the steel–UHPC composite beam has a relatively low growth rate with the increase in the load during the whole process of loading the steel–UHPC composite beam to the ultimate bearing capacity of the member. When the ultimate bearing capacity is reached, the stress values of the rebars of different components are all around 200 MPa, which is far from reaching the yield stress of the rebars. The role of reinforcement in steel–UHPC composite beams is smaller than that in steel–UHPC composite slabs.

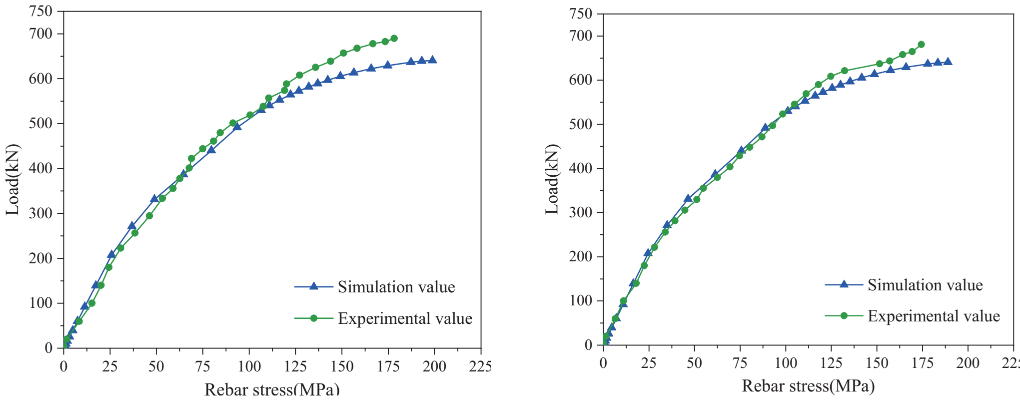

(**a**) U155-45-15-12. (**b**) U155-45-25-12.

Figure 13. Load-rebar stress curve for composite beams.

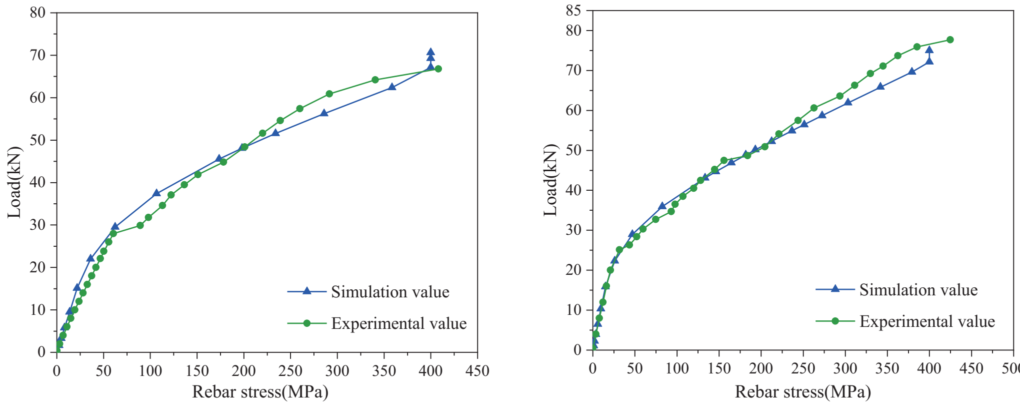

(**a**) S150-60-15-4. (**b**) S150-60-25-6.

Figure 14. Load-rebar stress curve for composite slabs.

3.4. Analysis of Key Design Parameters

Taking the composite slab as an example, based on the established ABAQUS finite element model, the effects of UHPC layer thickness, stud spacing, longitudinal reinforcement ratio, and protective layer thickness on the lateral bending performance of steel–UHPC composite slab are analyzed.

It can be seen from Figure 15 that with the increase in the thickness of the UHPC layer, the stiffness of each members from the linear elastic stage to the crack propagation stage is significantly improved, and the mechanical performance of the composite slab is significantly improved. The thickness of the UHPC layer greatly influences the initial stiffness of the steel–UHPC composite slab. With the increase in the thickness of the UHPC layer, the growth rate of the initial stiffness is gradually accelerated. This is because increasing the thickness of the UHPC layer can increase the bending moment of inertia of the section, the lateral bending deformation of the composite slab is slowed down, and the specimen's stiffness is also improved. From the variation law of the ductility reference index of each component shown in the figure, the thickness of the UHPC layer increases, and the bending flexibility of the composite slab becomes worse. When the thickness of the UHPC layer is between 40 mm and 55 mm, and between 60 mm and 70 mm, the ductility reference index decreases slightly, but when the thickness increases from 55 mm to 60 mm, the ductility index decreases greatly. The reason is that with the increase in UHPC thickness, the proportion of bearing capacity borne by UHPC layer gradually increases. When the thickness of UHPC increases from 55 mm to 60 mm, the reinforcement will soon reach the ultimate bearing capacity after yielding, there is little difference between the displacements corresponding to the ultimate bearing capacity and the yield load, so the ductility reference index decreases rapidly.

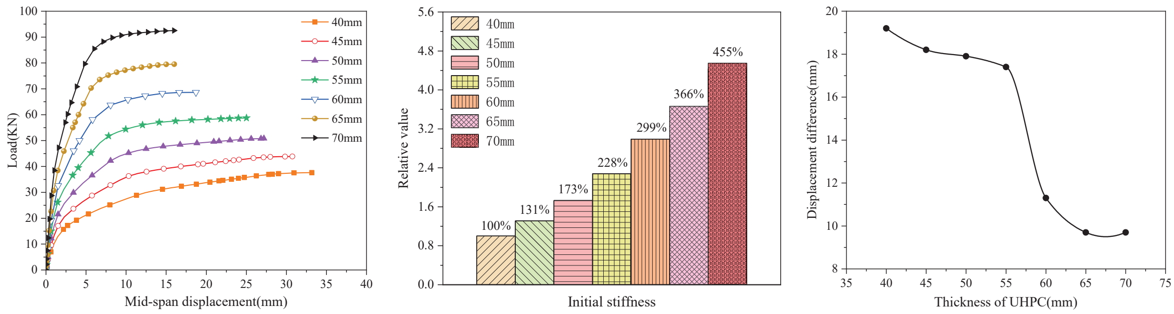

(a) Load-Mid-span displacement curve (b) Initial stiffness change (normalized) (c) Change of ductility reference index

Figure 15. Influence rule of variable UHPC layer thickness on composite board: (**a**) load-mid-span displacement curve, (**b**) Initial stiffness change (normalized), (**c**) Change of ductility reference index.

Figure 16 shows the influence of the calculated stud spacing on the load-mid-span displacement curve. The stud spacing has little effect on the initial stiffness of the composite slab. In the crack propagation stage, the composite slab stiffness increases with the decrease in the stud spacing, and the stiffness of the member with a stud spacing of 100 mm is significantly greater than that of the stud spacing greater than 100 mm specimens. This is because when the stud spacing is reduced, the number of studs increases, the shear resistance of the composite slab increases accordingly, and the ultimate bearing capacity of the component also increases with the decrease in the stud spacing. The stud mainly affects the stiffness and bearing capacity of the composite slab in the crack propagation stage and the yield stage. It can be seen from Figure 17 that the calculated reinforcement ratio has little influence on the initial stress in the elastic stage. In the crack propagation stage, the stiffness of the slab increases with the reinforcement ratio, that is, the reinforcement starts to play an obvious role from this stage. With the increase in load, cracks begin to appear on the surface of the UHPC layer and UHPC contains the disorderly distribution of steel fibers, which can limit the development of cracks and prevent them from being damaged. While it will exit the work quickly, and the force begins to transfer to the rebar, the tensile stress of the UHPC layer gradually decreases, and the stress of rebar increases rapidly at this stage. With the increase in the reinforcement ratio, the displacement increments of the member at the yield stage increases. Increasing the reinforcement ratio can effectively improve the bending flexibility of the composite slabs. Figure 18 shows the calculated load-mid-span displacement curves of composite slabs with different protective layer thicknesses. It can be seen that with the change of the thickness of the protective layer, the effect on the stiffness of the composite slab in the elastic stage is small, and the effect on the stiffness in the crack propagation stage and the ultimate bearing capacity in the yield stage is significantly increased.

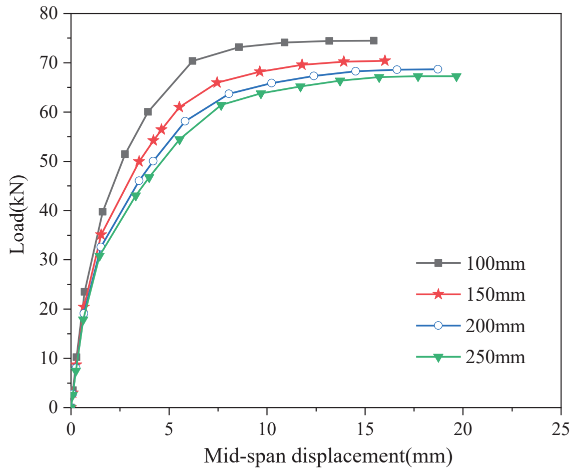

Figure 16. Load-mid-span displacement curves of composite slabs with different stud spacings.

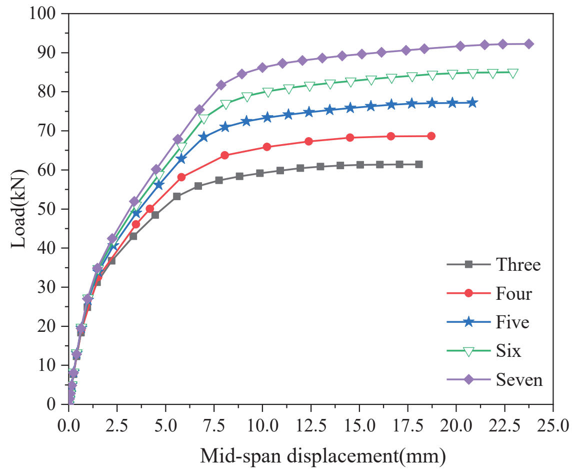

Figure 17. Load-mid-span displacement curves of composite slabs with different reinforcement ratio.

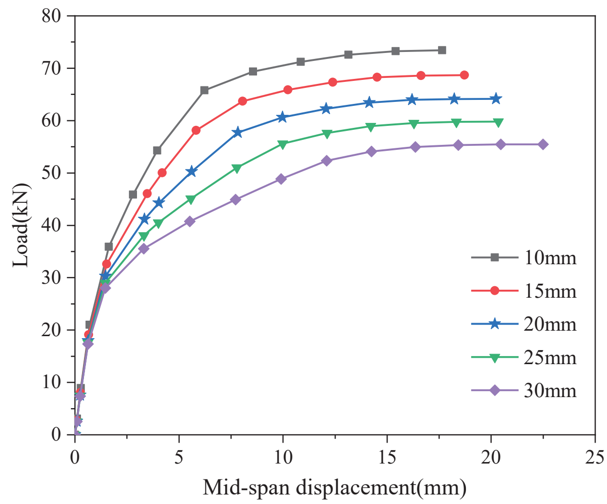

Figure 18. Load-mid-span displacement curves of composite slabs with different cover thickness.

For composite beams, Figure 19 shows the load-mid-span displacement curves of steel–UHPC composite beams with different U-rib thicknesses. It can be seen from the figure that with the increase in U-rib thickness, the stiffness of each member from the elastic stage to the crack propagation stage is significantly improved. This is because the U-rib can provide greater flexural rigidity, and increasing the thickness of the U-rib can significantly improve the mechanical performance of the composite beam. The thickness of the U-rib increased from 6 mm to 8 mm and 10 mm, respectively, and the ultimate bearing capacity increased by 35.5% and 70.0%, respectively, a relatively large increase. At the same time, the thicker the U-rib, the greater the displacement increment when the member is about to reach the yield failure stage, that is, the better elasticity of the composite beam.

The thickness of the UHPC layer has a certain influence on the stress state of the component in the whole processes. Because increasing the thickness of the UHPC layer can increase the overall height of the composite beam, increase the moment of inertia of the section, increase the bending stiffness, increase the bearing capacity, and improve the mechanical performance of the composite beam to a certain extent. However, the effect of the UHPC layer on the mechanical properties of the composite beam is much smaller than that of the composite slab because the contribution rate of the U ribs in the composite beam to the overall stiffness of the member is much greater than that of the UHPC layer. Different from composite slabs, with the increase in UHPC layer thickness, the flexural ductility deteriorates, and the mid-span displacement of each composite beam member when reaching the ultimate load changes very little; that is, the UHPC layer thickness has little effect on the composite beam ductility.

Figure 20 shows the influence of the thickness of the steel panel on the mid-span displacement curve of the steel–UHPC composite beam when the thickness of the U-rib is 6 mm. In the initial stage of loading, the thickness of the steel panel has little effect on the stiffness of the composite beam. After entering the stage of crack propagation, the structural stiffness changes with the increase in the thickness of the steel panel: when the thickness of the steel panel increases from 8 mm to 10 mm, the stiffness of the composite beam increases significantly, and the thicker the U rib, the greater the increase ratio. When the thickness of the steel panel increases from 10 mm to 16 mm, the stiffness of the composite beam only increases in a small range, and the changing trend could be clearer. At the same time, the thickness of the steel panel has little effect on the ultimate bearing capacity of each member.

Changing the thickness of the protective layer and the number of longitudinal reinforcements has little effect on the flexural performance of the composite beam. The reason is that compared with the steel–UHPC composite slab, the U-rib can provide greater bending stiffness for the composite beam, so during the loading process, the number of cracks on the upper surface of the UHPC layer in the pure bending section is relatively small. Moreover, the steel fibers distributed in UHPC will share part of the tensile stress, so the overall stress of the steel bar is low, that is, the role of the steel bar in the steel–UHPC composite beam is not obvious.

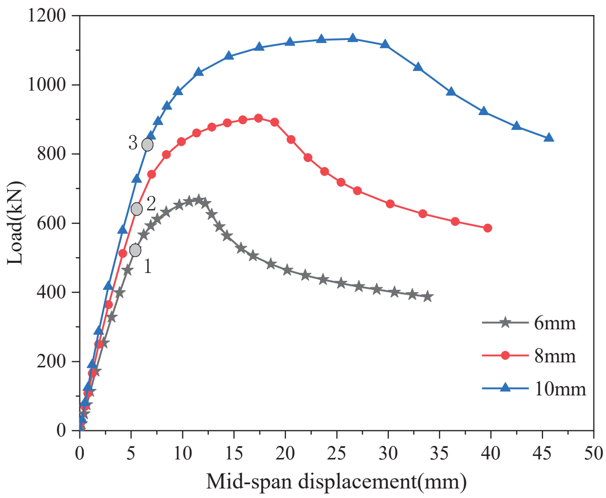

Figure 19. Load-mid-span displacement curves of composite beams with different U-rib thicknesses.

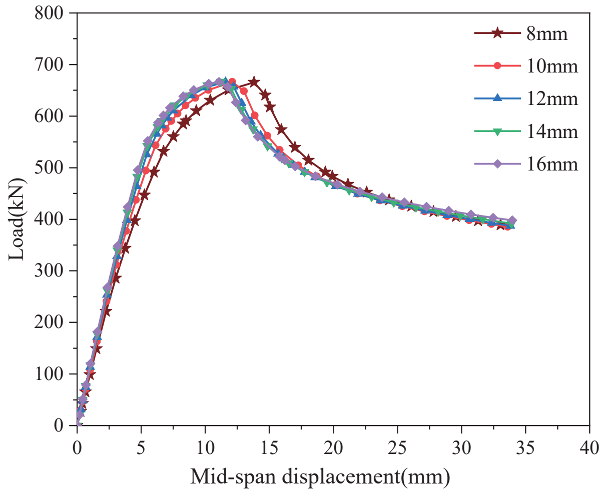

Figure 20. Load-mid-span displacement curves of composite beams with different steel plate thicknesses when the U-rib thickness is 6 mm.

4. Crack Load and Ultimate Bearing Capacity Calculation Theory

The calculation theory of the cracking load and ultimate bearing capacity of the steel–UHPC composite slab has been given in some studies, but there are few reports on the theoretical study of the mechanical properties of composite structures along the longitudinal bridge direction under the action of negative bending moment. Based on experimental research and finite element analysis, this paper deduces the theory of cracking load and ultimate bearing capacity of the steel–UHPC composite beam by using elastic–plastic theory and crack width calculation theory. The theoretical calculation formulas of the cracking load and ultimate bearing capacity of the steel–UHPC composite beam are deduced to provide a reference for the engineering design of the structure.

4.1. Calculation Theory of Cracking Load of Steel–UHPC Composite Beam

4.1.1. Crack Width Calculation

Studies have shown that the traditional method to calculate the cracking load of UHPC composite structures is too conservative [33,34]. At present, there are three main theories for calculating crack width, including no-slip theory, bond-slip theory, and comprehensive analysis theory combining no-slip and bond-slip. Based on these theories, various formulas for calculating the crack width of concrete have been put forward by codes around the world. To comprehensively consider the properties of UHPC materials and the bridging effect of steel fibers, this paper adopts the formula for calculating the crack width in the 2016 French Code [26], see Equations (5)–(12). The existing literature [35,36] also confirmed the applicability of this formula for calculating the crack width of steel–UHPC lightweight composite deck structures.

The formula for the crack width w_s around the reinforcement is:

$$w_s = s_{r,\max,f}\left(\varepsilon_{sm,f} - \varepsilon_{cm,f}\right) \tag{5}$$

$$s_{r,\max,f} = 2.55(l_0 + l_t) \tag{6}$$

$$l_0 = \frac{1.33c}{\delta} \tag{7}$$

$$\delta = 1 + 0.4\left(\frac{f_{ctfm}}{f_{ctm,el}K'_{global}}\right) \leq 1.5 \tag{8}$$

$$l_t = 2\left[0.3k_2\left(1 - \frac{f_{ctfm}}{f_{ctm,el}K_{global}}\right)\frac{1}{\delta\eta}\right]\frac{\phi}{\rho_{eff}} \geq \frac{l_f}{2} \tag{9}$$

$$\rho_{\text{eff}} = \frac{A_s}{A_{c,\,eff}} \tag{10}$$

$$\varepsilon_{sm,f} - \varepsilon_{cm,f} = \frac{\sigma_s}{E_S} - \frac{f_{ctfm}}{E_{cm}K_{global}} - \frac{1}{E_S}\left[k_t\left(f_{ctm,el} - \frac{f_{ctfm}}{K}\right)\left(\frac{1}{\rho_{eff}} + \frac{E_S}{E_{cm}}\right)\right] \tag{11}$$

The maximum crack width w_t on the UHPC surface is converted from the crack width around the steel bar:

$$w_t = \frac{w_s(h - x - x')}{(d - x - x')} \tag{12}$$

In the formula, $s_{r,\max,f}$ is the maximum crack spacing. $\varepsilon_{sm,f}$ is the average strain value of the reinforcement under consideration of the load combination. $\varepsilon_{cm,f}$ is the average strain value between UHPC cracks, and c is the thickness of the reinforcement cover. δ is the fiber reinforcement factor. $f_{ctm,el}$is the mean value of the elastic limits in tension of UHPC, f_{ctfm} is the mean value of the UHPC maximum stress after cracking, take 75% of $f_{ctm,el}$. K_{global} is the orientation coefficient of the longitudinal reinforcement (value range 1$\sim$2), take 1.75. K'_{global} is transverse reinforcement orientation factor. k_2 is the strain distribution factor considering the cracked section, the bending members is taken as 0.5. k_t is dependent on load duration or number of repetitions, the short-term load is taken as 0.6. ϕ is the rebar diameter, η is the bonding coefficient, and take 2.25. $l_f$is the longest fiber length. K is the fiber orientation coefficient. E_s is the elastic modulus of the steel. E_c is the elastic modulus of UHPC. ρ_{eff} is the effective reinforcement ratio. A_s is the steel bar area. $A_{c,eff}$is the effective cross-sectional area. σ_s is the steel bar stress. h is the total height of the section. d is the effective height of the section. x is the height of the compression zone of the section. x' is the height of the UHPC uncracked tension zone with tensile stress between 0 and $f_{ctm,el}$.

4.1.2. Crack Load Calculation

To simplify the calculation, the following assumptions are made for the cracking state of the steel–UHPC composition beam when the crack width reaches 0.05 mm: (1) due to the bridging effect of steel fibers, the UHPC layer located in the tension area can continue to provide tension after cracking. It is considered that the full section of the UHPC layer reaches the elastic limit tensile strength and remains unchanged. (2) The test results of steel–UHPC composite beams show that when a load of each member is before 77% to 86% of the ultimate bearing capacity, the strain distribution along the height direction of the section conforms to the assumption of a flat section. Therefore, under the action of cracking load, the assumption of the plane section is established, and the strain distribution of the section changes linearly. (3) The deformation is coordinated, and the longitudinal reinforcement strain is the same as the surrounding UHPC strain.

Based on the above assumptions, the internal force and bending moment balance equations of each section are deduced, as shown in Equations (13)–(22), and the corresponding steel stress obtained from the crack width formula when the maximum crack width of UHPC is 0.05 mm is substituted, and the solution is obtained. The height and curvature of the tensile zone of the section can be calculated to obtain the cracking moment of the composite beam, and then the cracking load can be obtained. Figure 21 shows the schematic diagram of cracking load calculation of steel–UHPC composite beam.

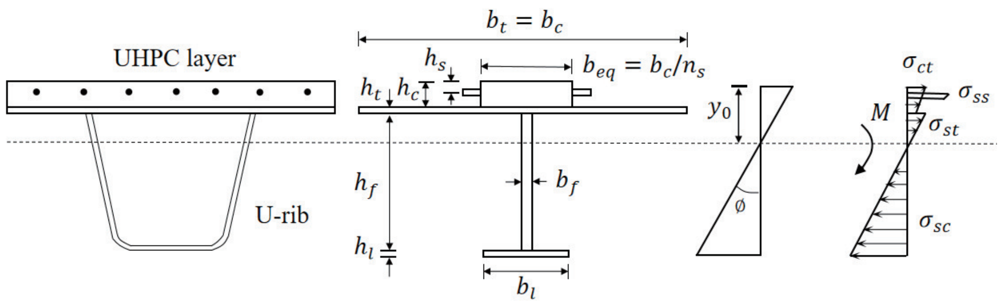

Figure 21. Schematic diagram of cracking load calculation of steel–UHPC composite beam.

The internal force N_{ct} and bending moment M_{ct} of the UHPC in the tension zone are expressed as:

$$N_{ct} = f_{ct} b_c h_c \tag{13}$$

$$M_{ct} = f_{ct} b_c h_c \left(y_0 - \frac{h_c}{2} \right) \tag{14}$$

The internal force N_{st} and bending moment M_{st} of the steel structure in the tension zone are expressed as:

$$N_{st} = b_t h_t E_s \varphi \left(y_0 - h_c - \frac{h_t}{2} \right) + b_f E_s \varphi \frac{(y_0 - h_c - h_t)^2}{2} \tag{15}$$

$$M_{st} = \frac{b_t E_s \varphi \left[(y_0 - h_c)^3 - (y_0 - h_c - h_t)^3 \right]}{3} + \frac{b_f E_s \varphi (y_0 - h_c - h_t)^3}{3} \tag{16}$$

The internal force N_{sr} and bending moment M_{sr} of the reinforcement in the tension zone are expressed as:

$$N_{sr} = A_s E_s \varphi (y_0 - h_s) = A_s \sigma_s \tag{17}$$

$$M_{sr} = A_s \sigma_s (y_0 - h_s) \tag{18}$$

The internal force N_{sc} and bending moment M_{sc} of the U-rib in the compression zone are expressed as:

$$N_{sc} = b_l h_l E_s \varphi \left(h_c + h_t + h_f - y_0 + \frac{h_l}{2} \right) + b_f E_s \varphi \frac{\left(h_c + h_t + h_f - y_0 \right)^2}{2} \tag{19}$$

$$M_{sc} = \frac{b_f E_s \varphi \left(h_c + h_t + h_f - y_0 \right)^3}{3} + \frac{b_l E_s \varphi \left[\left(h_c + h_t + h_f + h_l - y_0 \right)^3 - \left(h_c + h_t + h_f - y_0 \right)^3 \right]}{3} \tag{20}$$

The internal force and bending moment balance equation of each section under the action of external load are expressed as:

$$N_{sc} = N_{ct} + N_{st} + N_{sr} \tag{21}$$

$$M_{sc} + M_{ct} + M_{st} + M_{sr} = M_{cr} \tag{22}$$

In the formula, b_c and b_t are the width of the UHPC layer and the steel panel, respectively. E_c is the elastic modulus of UHPC, which is 45.8 GPa. E_s is the elastic modulus of steel, which is 206 GPa. y_0 is the distance from the section's neutral axis to the upper surface of the UHPC layer. h_c is the height of the UHPC layer. h_t is the height of the steel panel. h_s is the distance from the centroid of the longitudinal bar to the top surface of the UHPC layer. A_s is the area of the longitudinal bar. b_f and h_f are the U rib's web thickness and height after equivalent conversion, respectively. b_l and h_l are the width and height of the U-rib base plate, respectively. ϕ is the bending curvature of the section (1/mm). f_{ct} is the tensile strength of UHPC. M_{cr} is the cracking moment.

The cracking loads of composite beams obtained by theoretical calculation are compared with the experimental values, as shown in Table 3. The relative error between each component's calculated value and the test value is basically within 10%. Overall, the cracking load calculation formula proposed in this section has a certain accuracy, which can provide a reference for the designing the reinforced steel–UHPC composite deck structure.

Table 3. Cracking load of steel–UHPC composite beams.

Specimen	Calculated Value ①/KN	Test Value ②/KN	(②-①)/②
U55-45-15-12	486.9	538.4	9.6%
U55-45-25-12	399.7	437.0	8.5%
U55-60-15-12	481.6	492.5	2.2%
U55-60-25-12	447.3	439.8	−1.7%

4.2. Calculation Theory of Ultimate Bearing Capacity of Steel–UHPC Composite Beams

For the steel–UHPC composite beam studied in this paper, the test shows that when the ultimate bearing capacity of the structure is reached, the slip value between the steel panel and the UHPC layer of each component is very small, the maximum is only 0.035 mm, and the interface between the two remains largely intact. The bottom of the U-rib in the compression zone yielded, and the surface of the UHPC layer in the tension zone appeared to have fine cracks and developed to a certain height along the section. Due to the bridging effect of steel fibers, the UHPC did not quit work after cracking, the stress value of the steel panel was low, and the longitudinal rebars were far away unyielding. According to the test phenomenon and the stress characteristics of the steel–UHPC composite beam, the theoretical derivation of the calculation formula of the ultimate bearing capacity of the steel–UHPC composite beam is carried out by a simplified calculation method. Now assume the following:

(1) Under the ultimate stress state, the cracked UHPC in the tensile zone is considered to participate in stress 362 and keep the axial tensile strength unchanged.
(2) The flat section is assumed to be true, and the section strain distribution changes linearly.
(3) The bottom of the U-rib has yielded. The finite element model confirms that the rib also has a certain degree of yielding, but due to many unknown parameters, the yield height cannot be determined. The U-rib and the steel panel stress are assumed to be distributed in a triangle. At the same time, the actual yield strength of the Q345 steel used in the test is larger than the design yield strength, which is about 1.4 times the design yield strength. For the convenience of calculation and safety, the U -rib bottom reaches 1.2 times the yield strain for the calculation. In order to compare, the strain of the bottom of the U ribs is assigned ε_{sy} and $1.2\varepsilon_{sy}$, respectively. At this time, the calculation value of the corresponding combination beam limit bearing capacity N_{u1} and N_{u2}.

Based on the above assumptions, the ultimate bearing capacity of the steel–UHPC composite beam can be obtained from Equations (23)–(32).

The internal force N_{ct} and bending moment M_{ct} of the UHPC in the tension zone are expressed as:

$$N_{ct} = f_{ct} h_c b_c \tag{23}$$

$$M_{ct} = f_{ct} h_c b_c \left(y_0 - \frac{h_c}{2} \right) \tag{24}$$

The internal force N_{sr} and the bending moment M_{sr} of the reinforcement in the tension zone are expressed as:

$$N_{sr} = \frac{A_s E_s \varepsilon_S (y_0 - h_S)}{h - y_0} \tag{25}$$

$$M_{sr} = \frac{A_s E_S \varepsilon_S (y_0 - h_s)^2}{h - y_0} \tag{26}$$

The internal force N_{st} and bending moment M_{st} of the steel structure in the tension zone are expressed as:

$$N_{st} = \frac{b_t h_t E_s \varepsilon_s \left(y_0 - h_c - \frac{ht}{2}\right)}{h - y_0} + \frac{b_f E_s \varepsilon_s (y_0 - h_c - h_t)^2}{2(h - y_0)} \tag{27}$$

$$M_{st} = \frac{b_t E_s \varepsilon_S \left[(y_0 - h_c)^3 - (y_0 - h_c - h_t)^3\right]}{3(h - y_0)} + \frac{b_f E_s \varepsilon_S (y_0 - h_c - h_t)^3}{3(h - y_0)} \tag{28}$$

The internal force N_{sc} and bending moment M_{sc} of the U-rib in the compression zone are expressed as:

$$N_{Sc} = \frac{b_f E_S \varepsilon_S \left(h_c + h_t + h_f - y_0\right)^2}{2(h - y_0)} + \frac{b_l h_l E_S \varepsilon_S \left(h_c + h_t + h_f + \frac{h_l}{2} - y_0\right)}{h - y_0} \tag{29}$$

$$M_{sc} = \frac{b_f E_s \varepsilon_s \left(h_c + h_t + h_f - y_0\right)^3}{3(h - y_0)} + \frac{b_l E_s \varepsilon_s \left[\left(h_c + h_t + h_f + h_l - y_0\right)^3 - \left(h_c + h_t + h_f - y_0\right)^3\right]}{3(h - y_0)} \tag{30}$$

Under the action of ultimate bearing capacity, the balance equation of internal force and bending moment of each section are expressed as:

$$N_{sc} = N_{ct} + N_{st} + N_{sr} \tag{31}$$

$$M_{\max} = M_{sc} + M_{ct} + M_{st} + M_{sr} \tag{32}$$

$$F_{\max} = \frac{2M_{\max}}{L} \tag{33}$$

In the formula, h is the total height of the section; ε_s is the strain at the bottom of the U-rib, which is assigned ε_{sy} and 1.2 ε_{sy}, respectively, ε_{sy} is the design yield strain of the steel, which is 1675 $\mu\varepsilon$; L is the length of arm of force, which is 750 mm; $M_{\max}$ and $F_{\max}$ are the ultimate bending moments, respectively, and the ultimate bearing capacity; the meanings and values of the remaining parameters are the same as the formulae in Section 4.1.2.

The ultimate bearing capacity of the steel–UHPC composite beam calculated by the theoretical formula is compared with the experimental value and the finite element value, respectively, as shown in Table 4. It can be concluded that the result obtained from the calculated value N_{u1} is too small, and the relative error is relatively large. The reason is that the bottom of U-rib has yielded under the state of ultimate bearing capacity, and the actual yield strain of steel is larger than the standard yield strain, so this method is too conservative. The relative errors of each component in the calculated value N_{u2} are all within 10%. Overall, the calculation results of ultimate bearing capacity obtained by method N_{u2} have certain accuracy. The theoretical formula is relatively safe, which can provide a reference for the design of reinforced steel–UHPC composite deck structures.

Table 4. Ultimate bearing capacity of steel–UHPC composite beams.

Thickness of U Rids	Specimen	Calculated Value N_{u1}/kN	Calculated Value N_{u2}/kN	Test Value T/kN	FEM Value F/kN	$\frac{T(F)-N_{u1}}{T(F)}$	$\frac{T(F)-N_{u2}}{T(F)}$
6 mm	U155-45-15-12	543.3	642.2	690.3	/	21.3%	7.0%
	U155-45-25-12	539.7	637.8	683.0	/	21.0%	6.6%
	U155-60-15-12	565.1	664.9	705.4	/	19.9%	5.7%
	U155-60-25-12	560.8	659.6	639.0	/	12.2%	−3.2%
8 mm	U155-60-15-12	730.8	860.7	/	902.9	19.1%	4.7%
10 mm	U155-60-15-12	884.4	1043.0	/	1133.1	22.0%	8.0%

5. Conclusions

Based on experimental tests and FEM, this paper studies the influence of key design parameters, such as UHPC layer thickness, U-rib thickness, stud spacing, and reinforcement ratio on the longitudinal and transverse bending performance of steel–UHPC composite structures. In addition, calculation theories for predicting cracking load and ultimate bearing capacity are proposed. The main research contents and conclusions are as follows:

(1) The bending test results of steel–UHPC composite plates and steel–UHPC composite beams show that the load-mid-span displacement curve can be divided into three stages: elastic stage, crack propagation stage and yield stage. Fine and dense cracks appear on UHPC surface after failure of specimens.
(2) Non-linear FE models are established to study the influences of key design parameters on the flexural performance of the steel–UHPC composite slab. The results show that increasing the thickness of UHPC layer can significantly improve the stiffness and ultimate bearing capacity, but it has little effect on the cracking stress. Reducing the stud spacing can effectively reduce the slip value between UHPC layer and steel plate, and the shear–bending section studs play much larger role than the pure bending section studs. Increasing the longitudinal reinforcement ratio and reducing the cover thickness can increase the cracking stress and ultimate bearing capacity.
(3) Refined finite element models of steel–UHPC composite beams with different key design parameters were established and the influence law of key design parameters on the longitudinal bending performance of composite beam was analyzed. The results show that increasing the thickness of U-rib can significantly improve the stiffness and ultimate bearing capacity, and the flexibility of the composite beam is also better. Increasing the thickness of the steel plate has little effect on the ultimate bearing capacity and only increases the stiffness of the component in the crack propagation stage in a small range.
(4) The calculation theories for predicting the cracking load and ultimate bearing capacity of the steel–UHPC composite beam are proposed. The theoretical calculation values are in good agreement with the experimental values, and the finite element results and the errors are basically within 10%, which can be steel–UHPC light. Provide a reference for the engineering design of the composite bridge deck structure.

Author Contributions: Conceptualization, J.L.; Methodology, B.P.; Validation, Y.W.; Formal analysis, J.Z.; Investigation, L.Z. and Y.W.; Data curation, L.Z.; Writing—original draft, L.Z. and B.P.; Writing—review & editing, B.P. and H.Y.; Funding acquisition, J.L. All authors have read and agreed to the published version of the manuscript.

Funding: (1) the National Natural Science Foundation of China (grant No. 52008374); (2) the Natural Science Foundation of Hunan Province, China(grant No.2021JJ40593); (3) the Scientific and Technological Project of Henan Province, China (grant No.192102210185); (4) the Key scientific research projects of colleges and universities in Henan Province (grant No. 21A130002).

Data Availability Statement: Data available on request from the authors.

Acknowledgments: The authors would like to thank the following funders for their support to the studies in this paper: (1) the National Natural Science Foundation of China (grant No. 52008374); (2) the Natural Science Foundation of Hunan Province, China(grant No.2021JJ40593); (3) the Scientific and Technological Project of Henan Province, China (grant No.192102210185); (4) the Key scientific research projects of colleges and universities in Henan Province (grant No. 21A130002).

Conflicts of Interest: The authors declare no conflict of interest.

References

1. Cao, J.; Shao, X.; Deng, L.; Gan, Y. Static and fatigue behavior of short-headed studs embedded in a thin ultrahigh-performance concrete layer. *J. Bridge Eng.* **2017**, *22*, 04017005. [CrossRef]
2. Zhang, Y.S.; Li, F.X.; Xiong, F.; Zhou, X.D.; Li, W. Cause analysis and control measures of fatigue cracks in orthotropic steel deck. *J. Highw. Transp. Res. Dev.* **2013**, *30*, 75–80. (In Chinese) [CrossRef]
3. Li, X.; Chen, Y.; Zhou, Z.; Zhang, Q. New composite pavement structure on orthotropic steel bridge deck. *J. Highw. Transp. Res. Dev.* **2010**, *27*, 17–21.:SUN:GLJK.0.2010-01-005. (In Chinese) [CrossRef]
4. Dieng, L.; March, ; P.; Gomes, F.; Tessier, C.; Toutlemonde, F. Use of UHPFRC overlay to reduce stresses in orthotropic steel decks. *J. Constr. Steel Res.* **2013**, *89*, 30–41. [CrossRef]
5. Shao, X.; Yi, D.; Huang, Z.; Zhao, H.; Chen, B.; Liu, M. Basic performance of the composite deck system composed of orthotropic steel deck and ultrathin RPC layer. *J. Bridge Eng.* **2011**, *18*, 417–428. [CrossRef]
6. Shao, X.; Cao, J. Research and application of high performance bridge structures toward future. *J. Archit. Civ. Eng.* **2017**, *34*, 41–58. (In Chinese) [CrossRef]
7. Xuewei, W. *Study on Static and Fatigue Performance of Short Studs in Steel-UHPC Light Composite Bridge Deck*; Southwest Jiaotong University: Chengdu, China, 2017. (In Chinese)
8. Zheng, H. *Research on the Whole Process and Space Mechanical Performance of Steel-UHPC Light Composite Bridge Deck*; Hunan University: Changsha, China, 2016. (In Chinese)
9. Shen, X.J.; Brühwiler, E. Biaxial flexural fatigue behavior of strain-hardening UHPFRC thin slab elements. *Constr. Build. Mater.* **2020**, *255*, 119344. [CrossRef]
10. Shen, X.J.; Brühwiler, E.; Peng, W.H. Biaxial flexural response of Strain-Hardening UHPFRC circular slab elements. *Int. J. Fatigue* **2020**, *138*, 105727. [CrossRef]
11. Prem, P.R.; Murthy, A.R. Acoustic emission and flexural behaviour of RC beams strengthened with UHPC overlay. *Constr. Build. Mater.* **2016**, *123*, 481–492. [CrossRef]
12. Tanarslan, H.M.; Alver, N.; Jahangiri, R.; Yalçınkaya, Ç.; Yazıcı, H. Flexural strengthening of RC beams using UHPFRC laminates: Bonding techniques and rebar addition. *Constr. Build. Mater.* **2017**, *155*, 45–55. [CrossRef]
13. Noshiravani, T.; Brühwiler, E. Experimental investigation on reinforced ultra-high-performance fiber-reinforced concrete composite beams subjected to combined bending and shear. *ACI Struct. J.* **2013**, *110*, 251. [CrossRef]
14. Shao, X.; Zhang, Z.; Liu, M.; Cao, J. Research on bending tensile strength for composite bridge deck system composed of orthotropic steel deck and thin RPC topping. *J. Hunan Univ.* **2012**, *39*, 7–13. (In Chinese) [CrossRef]
15. Pei, B.; Li, L.; Shao, X.; Wang, L.; Zeng, Y. Field measurement and practical design of a lightweight composite bridge deck. *J. Constr. Steel Res.* **2018**, *147*, 564–574. [CrossRef]
16. Choi, W.; Choi, Y.; Yoo, S.W. Flexural design and analysis of composite beams with inverted-T Steel girder with ultrahigh performance concrete slab. *Adv. Civ. Eng.* **2018**, *2018*, 1356027. [CrossRef]
17. Li, W.; Shao, X.; Fang, H.; Zhang, Z. Experimental research on bending properties of steel-UHPC composite plates. *J. Civ. Eng.* **2015**, *48*, 93–102.:SUN:TMGC.0.2015-11-013. (In Chinese) [CrossRef]
18. Liao, Z.N.; Shao, X.D.; Qiao, Q.H.; Cao, J.H.; Liu, X.N. Static test and finite element simulation analysis of transverse bending of steel-ultra-high performance concrete composite slabs. *J. Zhejiang Univ. (Eng. Sci.)* **2018**, *52*, 1954–1963. (In Chinese) [CrossRef]
19. Luo, J.; Shao, X.; Cao, J.; Xiong, M.; Fan, W. Transverse bending behavior of the steel-UHPC lightweight composite deck: Orthogonal test and analysis. *J. Constr. Steel Res.* **2019**, *162*, 105708. [CrossRef]
20. Luo, J.; Shao, X.; Fan, W.; Cao, J.; Deng, S. Flexural cracking behavior and crack width predictions of composite (steel+UHPC) lightweight deck system. *Eng. Struct.* **2019**, *194*, 120–137. [CrossRef]
21. Wang, L.; Shao, X.; Cao, J.; Chen, Y.; He, G.; Wang, Y. Performance of steel-ultra-thin UHPC composite bridge deck based on ultra-short studs. *J. Zhejiang Univ. Eng. Ed.* **2020**, *54*, 2027–2037. (In Chinese) [CrossRef]
22. Nasrin, S.; Ibrahim, A. Finite-element Modeling of UHPC Hybrid Bridge Deck Connections. *Int. J. Adv. Struct. Eng.* **2018**, *10*, 199–210. [CrossRef]
23. Tzouka, E.; Karavasilis, T.; Kashani, M.M.; Afshan, S. Finite Element Modelling of Push-out Tests for Novel Locking Nut Shear Connectors. *Structures* **2021**, *33*, 1020–1032. [CrossRef]
24. Kmiecik, P.; Kamiski, M. Modeling of reinforced concrete structures and composite structures with concrete strength degradation taken into consideration. *Arch. Civ. Mech. Eng.* **2011**, *11*, 623–635. [CrossRef]
25. Yan, P.Y.; An, M.Z.; Du, Q.; Huang, Z.Y.; Wang, B.; Zhou, Y.X.; Huang, Z.J.; Song, S.M.; He, K.; Ji, W.Y.; et al. *Reactive Powder Concrete (GB/T 31387-2015)*; Ministry of Housing and Urban-Rural Development of People's Republic of China: Beijing, China, 2015. Available online: https://max.book118.com/html/2019/0106/5024341001002000.shtm (accessed on 1 November 2015). (In Chinese)
26. AFNOR. *National Addition to Eurocode 2—Design of Concrete Structures: Specific Rules for Ultra-High Performance Fibre-Reinforced Concrete (UHPFRC)*; Association Francaise de Normalisation: Paris, France, 2016. Available online: http://uhpc.com.vn/wp-content/uploads/2018/09/NF-P-18-710-UHPC.pdf(accessed on 16 April 2016).
27. Li, J. *Research on Mechanical Properties of Lightweight Aggregate Concrete stud Connectors Based on Damage Effect*; Beijing Jiaotong University: Beijing, China, 2020. (In Chinese)

28. Zhao, M.; Huang, F.; Liu, Q.; Qiu, M.; Huang, Z.; Hu, W.; Shao, X. Finite element analysis of steel plate-ultra-high performance concrete beams. *China Concr. Cem. Prod.* **2021**, *297*,67–71. . (In Chinese) [CrossRef]
29. Zhuang, Z. *Finite Element Analysis and Application Based on ABAQUS*; Tsinghua University Press: Beijing, China, 2009. (In Chinese)
30. Zeng, Y.; Hu, L. Calculation transformation and calibration of ABAQUS concrete plastic damage constitutive model. *Water Resour. Power* **2019**, *37*, 106–109. (In Chinese) [CrossRef]
31. Yang, J.; Fang, Z. Research on stress-strain relation of ultra high performance concrete. *China Concr. Cem. Prod.* **2008**, *7*, 11–15. (In Chinese) [CrossRef]
32. Wang, Y. *ABAQUS Structural Engineering Analysis and Detailed Example*; China Construction Industry Press: Beijing, China, 2010. (In Chinese)
33. Genders, W.; Razavi, S. Asynchronous n-step Q-learning adaptive traffic signal control. *J. Intell. Transp. Syst.* **2019**, *23*, 319–331. [CrossRef]
34. Zlatkovic, M.; Zhou, X. Effective Coupling of Signal Timing Estimation Model and Dynamic Traffic Assignment in Feedback Loops: System Design and Case Study. 2014. Available online: https://trid.trb.org/view/1289695 (accessed on 16 January 2014).
35. Luo, J.; Shao, X.; Cao, J.; Fan, W.; Pei, B. Orthogonal test and calculation method of cracking load of steel-ultra-high performance concrete composite specimen. *J. Zhejiang Univ. (Eng. Sci.)* **2020**, *54*, 909–920. Available online: https://www.zjujournals.com/eng/CN/article/downloadArticleFile.do?attachType=PDF&id=41342 (accessed on 1 May 2020).
36. Zhou, X.; He, Y.; Liu, R.; Xue, M.; Wang, X. Study on calculation method of crack width for steel-UHPC composite Beam cable-stayed bridge panel. *Highw. Eng.* **2021**, *46*, 110–117. (In Chinese) [CrossRef]